TAO, Vol.2, No.2, PP. 121-146, June 1991

Observational Study of a Multiple Microburst-Producing Storm Part II: A Comparison Between the Simple Case and the Complex Case

YEONG-JER LIN[1] AND JOHN A. COOVER, JR.[2]

(Received 13 March 1991; Revised 29 July 1991)

ABSTRACT

A cross-comparison in structure and internal dynamics was made between a single microburst-producing storm (the simple case) and a multiple microburst-producing storm (the complex case) in Colorado. Emphasis was placed on the observed features in the atmospheric boundary layer (ABL) where the microburst activities dominated. In each case, the dual-Doppler derived winds and retrieved thermodynamic variables at two analysis times were employed to conduct the study.

Results show that there are similarities and differences in structural features between the two cases. Similar features found include: (1) the microbursts being investigated were embedded within the high-reflectivity regions with precipitation occurrence; (2) a wet microburst is accompanied by the bow echo with the outflow in the direction parallel to the maximum reflectivity gradient; (3) high pressure forms inside the microburst core with low pressure in the strongest outflow regions; (4) a rotor forms near the microburst gust front due to the outflow colliding with the environmental flow; (5) a net eddy transfer of horizontal momentum and kinetic energy in the microburst area is predominantly downward; and (6) the pressure and buoyancy effects are two main contributors to the generation/decay of horizontal momentum fluxes and eddy kinetic energy at the microburst levels. On the other hand, different features between the cases are (1) each case has unique environmental ingredients, such as the wind, vertical shear, stability, and moisture; (2) the environmental mean flow in the ABL is opposite in direction (southeast versus northwest); (3) a strong (weak) downflow occurs in the main downdraft for the simple (complex) case; (4) only one microburst occurs in the simple case, while at least two microbursts occur in the complex case at each analysis time; (5) no apparent circulation center is found in the simple case, while the complex case has the mesocyclone-like vortex and misocyclones; and (6) a wet microburst has a warm (cold) core for the simple (complex) case.

---

[1] *Department of Earth and Atmospheric Sciences, Saint Louis University, U. S. A.*

[2] *Air Weather Service, U. S. Air Force.*

1. INTRODUCTION

In Part I of this study, Lin *et al.* (1991) investigated kinematic, dynamic, and thermodynamic structures of a multiple microburst-producing storm in Colorado using dual-Doppler data collected at 1845, 1847 and 1850 MDT analysis times. This storm occurred on 5 August 1982 within the JAWS network and produced at least two microbursts during each analysis times. For convenience, it is referred to as the complex case in this study. The data sets were only available in the atmospheric boundary layer (ABL) due to the shallow layer scans. These data were judiciously analyzed to produce a detailed wind field in the horizontal domain of 15 *km* by 15 *km*. Once the three-dimensional wind field was derived, fields of deviation perturbation pressure and temperature were obtained from the three momentum equations using a thermodynamic retrieval method (Gal-Chen, 1978). Results showed that the microbursts were embedded within the high-reflectivity cores of heavy precipitation. A wet microburst below 0.75 *km* was accompanied by the misocyclone at levels above 0.75 *km* in the main downdraft. The slowly descending downflow formed a cold core at the lowest levels due to the evaporation of raindrops. Near the gust front (GF), a mesocyclone-like circulation developed in the area where the warm, dry environmental air interacted with the negatively buoyant microburst outflow. High pressure formed inside the microburst core with low pressure in the strong wind regions. The retrieved pressure and temperature fields agreed well with the storm's kinematic structure. The combined effects of misocyclone circulations, perturbation-pressure gradients, buoyancy and precipitation loading were responsible for maintaining the microburst downdrafts in the ABL.

Using the Doppler derived winds and retrieved thermodynamic variables for the same case at 1845 and 1850 MDT 5 August, 1982, Lin and Coover (1990) investigated budgets of horizontal momentum fluxes and eddy kinetic energy. Results showed that the microburst activities in the ABL enhanced eddy transfer processes of horizontal momentum and kinetic energy, especially in the areas of strongest downflowing air. The presence of a mesocyclone-like circulation at low levels and the micocyclones aloft contributed to the vertical transport of horizontal momentum and eddy kinetic energy. In the sub-domain of a microburst, the net transfer of horizontal momentum and eddy kinetic energy was predominantly downward through the whole boundary layer. Magnituded of the net transfer were directly related to the microburst strength at the time of analysis. The pressure and buoyancy effects were the two major contributors to the horizontal momentum-flux and eddy kinetic energy budgets. These two terms had the same order of magnitude but opposite sign at the lowest levels where the microbursts dominated.

Structural features, horizontal momentum-flux and kinetic energy budgets

of a microburst-producing storm at 1647 MDT 14 July 1982 were reported in studies by Lin and Hughes (1987), Lin *et al.* (1987), Lin and Condray (1988) and Lin (1988). This storm produced only one microburst during the storm's entire life span and is referred to as the simple case hereafter. Results showed that the single microburst was embedded within the high-reflectivity region of precipitation. A strong downflow impinged on the surface, producing a stagnation mesohigh inside the microburst. This high was accompanied by low pressure in the strongest outflow regions, forming a pronounced horizontal pressure gradient outward from the high-pressure center. Such pressure patterns were in good agreement with the surface observations in similar cases for two different storms. The microburst had a warm-core structure since the rapidly descending downflow air can warm up dry-adiabatically all the way to the ground. This finding agreed well with that reported in Fujita (1985) for Colorado microbursts. The outflow region extended from the surface to approximately 1 km with maximum divergence in excess of $10^{-2}\ s^{-1}$. The outflow air was negatively buoyant due to evaporation in the outskirt of the microburst. The retrieved buoyancy field matched well with the updraft-downdraft structure and the pressure pattern. The combined effects of perturbation-pressure gradients, buoyancy and precipitation loading were responsible for maintaining the downdrafts which produced the strong diverging outflow at low levels. The microburst occurrence in the ABL enhanced eddy transfer of horizontal momentum and eddy kinetic energy. A net transfer of horizontal momentum and eddy kinetic energy was downward toward the surface due to the organized downdrafts. The generation/decay of horizontal momentum-flux and eddy kinetic energy at the microburst levels was mainly determined by the pressure and buoyancy effects. These two terms were nearly in balance, having the same order of magnitude but opposite sign.

The purpose of this study in Part II is to compare the findings obtained for the complex case (5 August 1982) to those for the simple case (14 July 1982) mentioned previously. To add to the discussion and comparison, an additional data set at 1649 MDT 14 July 1982 for the simple case is added to the investigation in Part II of this study. Throughout a systematic comparison and cross-comparison, some similarities and differences in structure and internal dynamics between the two cases can be researched in detail. Finally, the hypothesized conceptual model of a microburst for each case, based on the observational evidences, is presented. The goal is to better understand the relevant physical processes which govern and maintain the microburst activities in the ABL at the times of interest.

2. DATE AND ANALYSIS PROCEDURES

The synoptic situation at 0600 MDT 14 July 1982 (Fig. 1) revealed a cold front located to the northwest of Colorado. The Denver area was in the warm

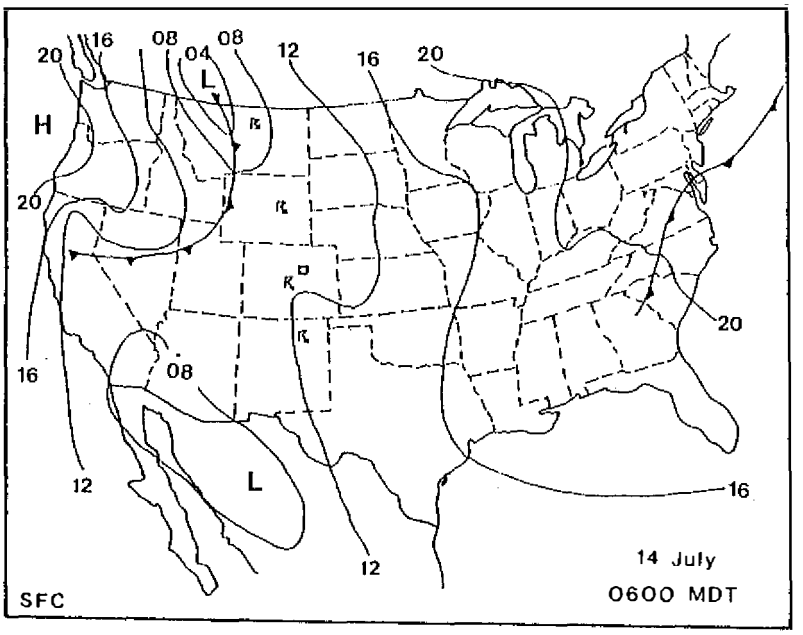

Fig. 1. The surface synoptic map at 0600 MDT 14 July 1982. The small box located in the state of Colorado indicates the JAWS area.

sector and was under the influence of unstable air. The front passed through the Denver area around 1800 MDT, triggering widespread convertive activities. For comparison, the Denver sounding released at 1800 MDT for the simple case is plotted against that released at 1800 MDT for the complex case in Fig. 2. For the simple case (thin lines), a dry air extended from the surface to 3.5 *km* AGL, characteristic of the atomspheric environment in the Denver area during the summer season. The lapse rate was nearly dry adiabatic from the surface to 600 *mb*. A shallow moist layer from 500 to 450 *mb* was observed with a slight inversion at 450 *mb*. An unmixed parcel lifted moist-adiabatically from 530 *mb* would buoyantly ascend to 280 *mb* ($\approx$ 8 *km* AGL). The height of the dry air corresponds well with the reported cloud base at 3.5 *km*. On the other hand, the Denver sounding for the complex case (heavy lines) features a well-mixed boundary layer, extending from the surface to 1.5 *km* AGL. The lefting condensation level (LCL) was 650 *mb* ($\approx$ 2 *km* AGL) as compared to 3.5 *km* for the simple case, indicating a relatively moist air in the lower troposphere. Note the unusual depth of the moist layer (4 $\sim$ 7 *km*) for a high plains storm and the general lack of mid-level dry air. A cross-comparison between the two soundings reveals that the complex case had relatively high mixing ratio (6.5 g/kg, a deeper moist layer (3 *km*), and winds backing with height in the lower layer. Conversely, the simple case had a much lower mixing ratio (4.5 g/kg), a shallow moist layer (1.5 *km*) and little directional shear in the ABL. In the middle and upper layers, the complex case has much stronger winds and vertical shear than

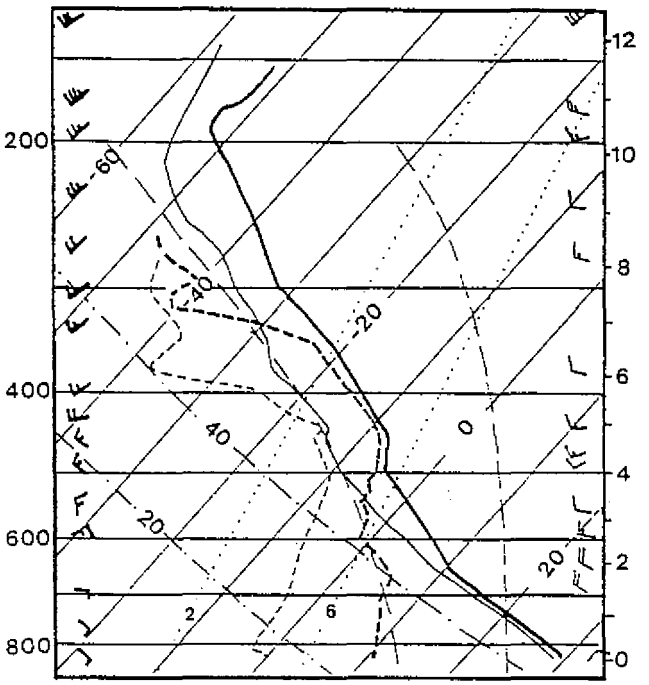

Fig. 2. The Denver soundings released at 1800 MDT 5 August 1982 (heavy lines), and at 1800 MDT 14 July 1982 (thin lines). A solid line represents temperature, while a dashed line denotes dew point temperature. Heights are in kilometers AGL. Environmental winds shown on the extreme right (left) are associated with the simple (complex) case.

those for the simpler case. Apparently, the environmental conditions between the two cases are quite different.

The data analysis and reduction procedures for the complex case have been detailed in Part I of this study. In the following, only the data and analysis procedures for the simple case at the 1649 MDT analysis time are briefly described.

Dual-Doppler data, obtained from CP-3 and CP-4, were objectively analyzed in the domain with horizontal dimensions of 10 *km* by 10 *km* centered on the microburst. Only those data with a high signal-to-noise ratio were accepted for analysis. The cell motion at the time of analysis was nearly stationary. The objective analysis scheme of Barnes (1973) was expanded from two-dimensional to three-dimensional. All variables within a slab were interpolated onto horizontal Cartesian grids (20×20) using a 1.75 *km* scan radius. Unlike the 1647 MDT data set used by Lin and Hughes (1987) for the whole storm volume, dual-Doppler data collected at 1649 MDT were confined to a shallow layer from the surface to 2 *km*. There were six analysis levels in the vertical from 0.25 to 2 *km* covering the entire ABL. The horizontal grid spacing was 0.5 *km*, while the vertical grid spacing varied from 0.25 *km* for the levels below 1 *km* to

0.5 *km* for those above 1 *km*. We employed two radial velocity equations, the anelastic continuity equation, and an empirical formula of terminal fall speed to obtain the horizontal wind components (u, v). The vertical verocity component (w) was computed from the anelastic continuity equation by integrating upward from the surface assuming $w = 0$ at the surface. Subsequently, fields of deviation perturbation pressure and temperature were retrieved from the three momentum equations as depicted in Part I, Section 3.

3. DISCUSSION OF RESULTS

3.1 Structural Features for the Simple Case

In the following discussion, emphasis is focused on the structure and internal dynamics of a single microburst-producing storm at 1649 MDT on 14 July 1982. Remember this analysis time was not included in our earlier studies for the same storm mentioned previously.

Figure 3 shows the horizontal storm-relative wind fields at 0.25, 0.75, and 1.5 *km*. Heights are in kilometers AGL and distances are in kilometers from the CP-2 radar (see Fig. 3 in Part I). Contours of radar reflectivity in 5 *dBZ* increments are superimposed on the wind fields. Line AB in Fig. 3a signifies the cross sections presented later. At 0.25 *km* (Fig. 3a), a pronounced microburst diverging flow extends from the microburst center (M), located at ($x = -12$, $y = -18$), outward in all directions. The microburst core is located in the bow echo and embedded within the high-reflectivity region with $Z > 45$ *dBZ*. A strong microburst gust front (dashed line), abbreviated GF hereafter, is located northeast of the center (M), while a weak GF is located west and northwest of M. The strongest winds occur between M and the GF on the east side of the microburst core. These strong winds coincide with the location of Standley Lake, Colorado. At the eastern edge of the strong wind regions, an area of strong convergence occurs in a region of low reflectivities associated with the environmental airflow. Note that the strong outflow is almost parallel to the maximum reflectivity gradient. Such features are also found in the complex case at 0.25 *km* (see Figs. 4a and 5a in Part I), especially in the M1 microburst area. At 0.75 *km* (Fig. 3b), the GF to the east of M is still apparent. However, the outflow has weakened considerably at this level. The weak GF northwest of M is still intact. This gust front is caused by the dynamical interaction between the negatively buoyant microburst outflow and the incoming environmental flows as depicted in Lin and Hughes (1987). In the area along the GF, upward motion prevails. Its magnitude is directly proportional to the strength of the microburst outflow and environmental flow. The 1.5 *km* horizontal wind pattern (Fig. 3c) reveals that the strong outflow region east of M, noted earlier at low levels, is almost lost. Strong winds begin to develop to the west of the bow echo.

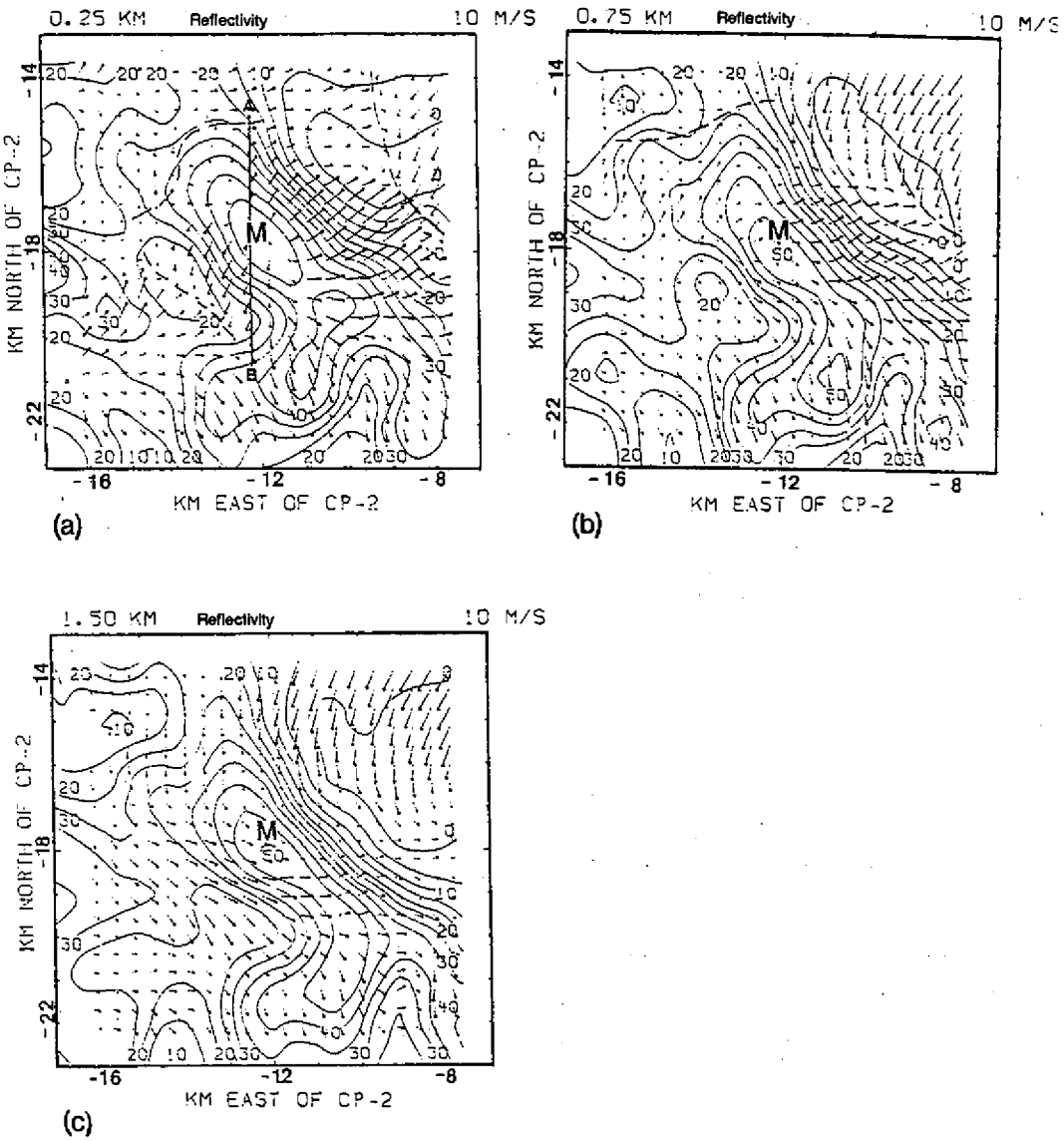

Fig. 3. Horizontal storm-relative wind fields with reflectivity contours superimposed at (a) 0.25, (b) 0.75, and (c) 1.5 *km* for the simple case at 1649 MDT 14 July 1982. Distances are in kilometers from CP-2. The dashed line represents the gust front (GF). The microburst center at 0.25 *km* is labeled M. Line AB in panel (a) signifies the cross sections presented in Figs. 7 to 9.

The strong west-northwest wind maximum occurs near (−12, −19) with strong confluence to its north and northeast, and diffluence to its south and southeast. The large decrease in magnitude of the horizontal wind at this level suggests that some mass has to be transported downward just southeast of the 50 dBZ contour located in the microburst head. The vertical velocity field (not shown) shows a large area of downward motion located where the horizontal winds

are diverging outward from the wind maximum across the bow echo in the high-reflectivity region. The reduction in horizontal wind speed across the bow echo at the microburst location, with a corresponding increase in downward motion, confirms that some of the dry, high-speed, environmental air injected into the bow echo mixes with the nearly saturated downdraft and enhances the microburst at low levels. Lin and Condray (1988) showed that horizontal momentum fluxes are directed downwared in the microburst downdraft column for the simple case at 1647 MDT.

Inspection of Fig. 3 further reveals that there is no apparent mesocyclone-like circulation at 0.25 *km* and levels above. Similarly, no misocyclone occurs at 0.75 and 1.5 *km*. As a result, values of vertical vorticity are relatively small at all levels (not shown). Further, no well-defined vorticity center is found at any level. On the contrary, both the mesocyclone-like vortex and misocyclones are observed in the complex case at 1845 and 1850 MDT (see Figs. 4 and 5 in Part I), resulting in large values of vertical vorticity. Table 1 shows the maximum values of vertical vorticity (ζ_{max}) at centers of the mesocyclone-like vortex and misocyclones at 1845, 1847 and 1850 MDT. Positive values signify cyclonic vorticity and vice verse. Note that value of ζ_{max} increase substantially as the misocyclones intensify at 1850 MDT. In particular, the magnitude of maximum vertical vorticity for the M2 misocyclone at 1850 MDT is about two times larger than that at 1845 MDT. Conversely, the mesocyclone-line vortex decreases its circulation slightly at 1850 MDT as compared to that at 1845 MDT. This is attributed to the appearance of M3 at 1850 MDT detailed in

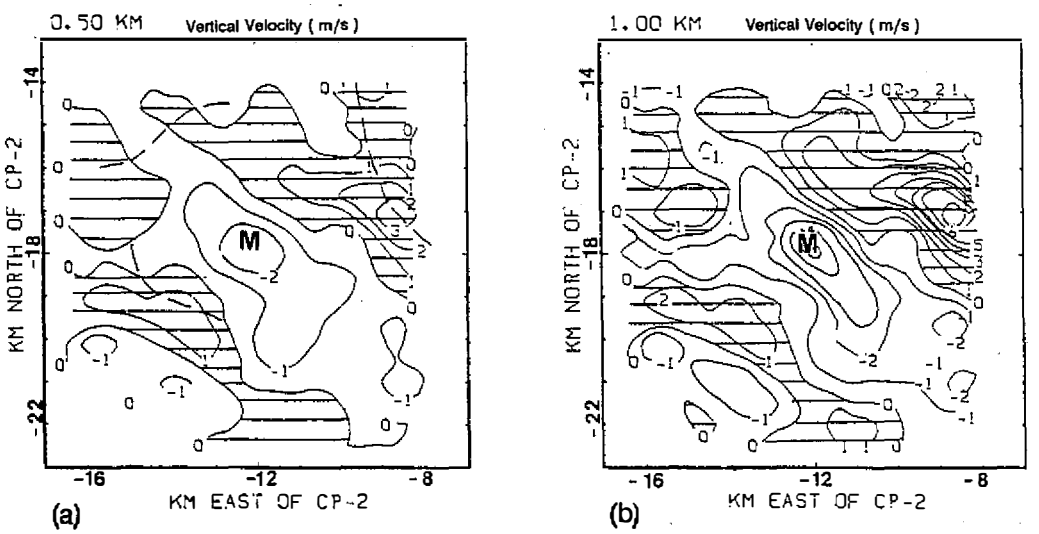

Fig. 4. Horizontal distributions of vertical velocity in meters per second at (a) 0.5, and (b) 1 *km* for the simple case at 1649 MDT. Contour interval is 1 *m/s* with positive values hatched. The microburst center (M) at 0.25 *km* is marked. The dashed line represents the gust front (GF).

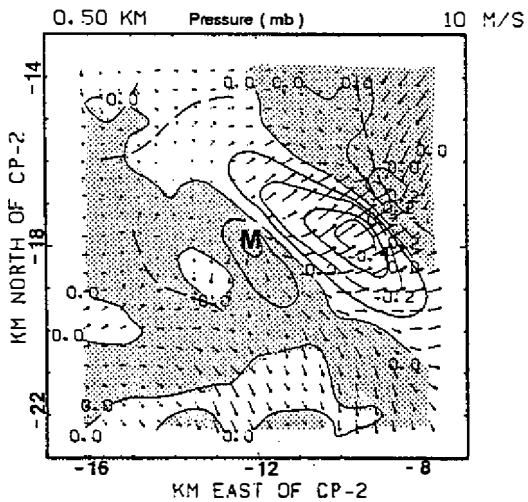

Fig. 5. The distribution of deviation perturbation pressure in hPa (mb) at 0.5 km for the simple case at 1649 MDT. Contour interval to 0.1 mb with positive values shaded. Horizontal storm-relative winds are superimposed. A symbol M signifies the microburst center at 0.25 km. The dashed line represents the gust front (GF).

Table 1. Maximum values of vertical vorticity (ζ_{max}) at centers of the mesocycone-like vortex and misocyclones for the complex case at 1845, 1847 and 1850 MDT 5 August 1982. Units are in 10^{-3} s^{-1}. A positive value signifies cyclonic vorticity.

	Mesocyclone-like vortex				M1 misocyclone				M2 misocyclone			
z (km)	1845	1847	1850	MDT	1845	1847	1850	MDT	1845	1847	1850	MDT
0.25	13.0	10.5	8.1		–	–	–		–	–	–	
0.50	14.6	11.4	8.3		–	–	–		–	–	–	
0.75	10.2	10.9	11.7		7.7	9.1	10.8		6.7	10.0	13.4	
1.00	14.5	12.6	11.1		9.8	11.3	12.7		7.3	10.3	13.5	
1.25	7.9	6.1	4.7		11.5	12.7	14.3		7.4	11.3	15.1	

Part I of this study. In Part III, the generation/decay of vorticity for both cases will be investigated in detail. Examination of Fig. 3 further reveals that the prevailing flow for the simple case is from the north and northwest; whereas, the prevailing flow is from the south and southeast or the complex case.

Horizontal distributions of vertical velocity at 0.5 and 1 km for 1649 MDT are presented in Fig. 4. At 0.5 km (Fig. 4a), downward motion dominates in the microburst area with maximum velocity coincident with the microburst center (M). The downdraft is surrounded by upward motion outside of the microburst area. Such upward motion is caused by the interaction between the microburst outflow and the environmental flow, and is coincident with the positions of microburst gust fronts (dashed line). The strongest updraft with maximum

speed $> 3\ m/s$ occurs along the strong GF near $(-8.5, -17)$. A secondary updraft with much weaker vertical velocity ($1\ m/s$) forms in the area southwest of the weak GF. Both upward and downward velocities increase considerably at 1 km (Fig. 4b). The maximum downdraft speed now reaches $-5\ m/s$. This magnitude is more than two times larger than that for the complex case at the same height (see Figs. 6b and 7b in Part I). The updraft on the east side of M has intensified with maximum speed in excess of $5\ m/s$, while the updrafts on the west side of M along the GF remain weak due to weak forcing at levels below.

As described in Part I, the pressure field is calculated from the horizontal pressure equation using the Doppler derived winds. The retrieved field is subjected to momentum checking to determine the level of confidence. Such checking provides a relative error, E_r, in pressure retrieval. Smaller values of E_r (< 0.5) are desirable since they represent a good balance between the wind fields and the retrieved horizontal perturbation-pressure gradients. Values of E_r for the simple case at 1649 MDT are presented in Table 2. For comparison, values of E_r for the complex case at 1845, 1847 and 1850 MDT are also presented. Notice that in the layer below 1 km, where the microburst dominates, relative errors (E_r) are comparably smaller than those in the layer aloft. A cross-comparison between the two cases reveals that the simple case, as a whole, has smaller E_r values than those for the complex case at most levels. This result is reasonable since the flow field in a single microburst-producing storm is far less complicated than that observed in a multiple microburst-producing storm.

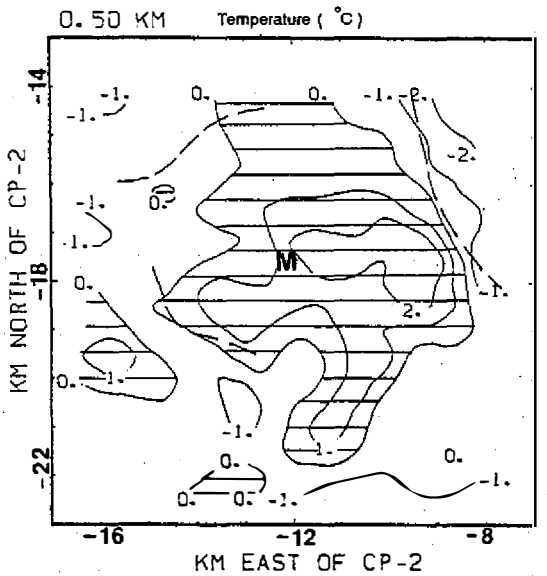

Fig. 6. The distribution of deviation perturbation temperature in $°C$ at 0.5 km for the simple case at 1649 MDT. Contour interval is $1°C$ with positive values hatched.

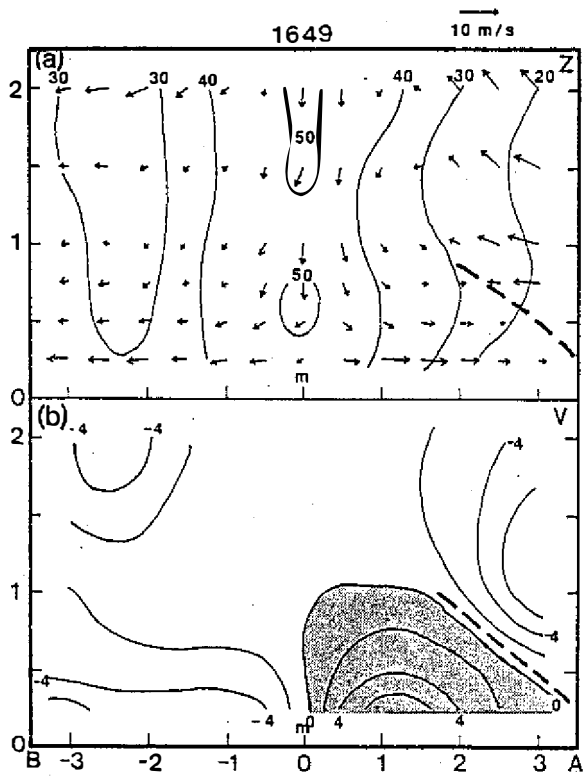

Fig. 7. The cross section along line AB in Fig. 3a showing (a) the storm-relative wind with reflectivity (Z) superimposed, and (b) the V-component for the simple case at 1649 MDT. Contour interval is 10 dBZ for Z and is 2 m/s for V with positive values (northward) shaded. The microburst center (M) near the ground is marked. The heavy dashed line represents the gust front (GF). Distances are in kilometers from the microburst center (M).

Table 2. Results of momentum checks (E_r) for the simple case (14 July 1982) at 1649 MDT and the complex case (5 August 1982) at 1845, 1847 and 1850 MDT.

	Simple case		Complex case			
z (km)	1649	MDT	1845	1847	1850	MDT
0.25	0.19		0.29	0.20	0.28	
0.50	0.15		0.38	0.34	0.38	
0.75	0.23		0.40	0.38	0.39	
1.00	0.36		0.38	0.34	0.34	
1.25	–		0.40	0.32	0.39	
1.50	0.30		–	–	–	
2.00	0.21		–	–	–	
Average	0.24		0.37	0.32	0.36	

For this reason, a better balance between the horizontal pressure gradients and the observed wind fields is likely to achieve for the simple case.

Figure 5 depicts the retrieved field of deviation pressure (P'_d) at 0.5 km for 1649 MDT. Storm-relative winds are superimposed on the pressure field. Note that high pressure (0.2 mb) forms inside the microburst inner core region with low in the strong outflow regions. The large horizontal pressure gradient east of M is consistent with the acceleration of air to the east. Another weaker low pressure area to the west of the microburst coincides with the weak GF. Pronounced horizontal perturbation-pressure gradients are directed outward from the high pressure center at the microburst core (M) to the surrounding low pressure areas. Such pressure gradients are needed in order for the storm to maintain the accelerated flow associated with the microburst outflow, especially in the area east of M. The pressure pattern seen in Fig. 5 is quite comparable with that observed two minutes earlier for the same case reported in Lin *et al.* (1987), see their Fig. 8. Furthermore, horizontal pressure gradients for the simple case are much greater than those for the complex case (see Fig. 8 in Part I). This is mainly attributed to the difference in structure and intensity between the two microburst system under comparison.

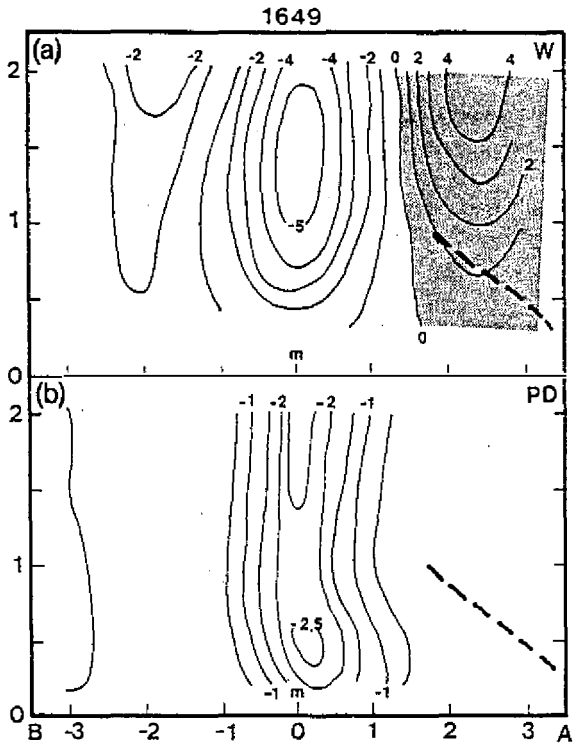

Fig. 8. The cross section along line AB in Fig. 3a showing (a) vertical velocity (w), and (b) precipitation drag (PD). Contour intervals are 1 m/s and 0.5×10^{-2} $m/s/s$ (with positive values shaded) for w and PD, respectively.

The simple microburst case is characterized by a warm core (Fig. 6). This feature is consistent with results obtained by Lin and Hughes (1987) for the same case except for 1647 MDT. Fujita (1985) found that the air temperature in a microburst can be either warmer or colder than its environment. In a wet microburst with a strong downflow, such as the case being investigated here, the air temperature is likely to be warmer than its surrounding. He explained that downflow air can warm up dry-adiabatically all the way to the ground, unless embedded raindrops can evaporate fast enough to maintain a moist-adiabatic descent. On the other hand, the temperature excess to the east of M in the microburst outskirt coincides with the strongest outflow in the deepest low pressure area (Fig. 5). The vertical perturbation-pressure gradient there is predominantly downward, resulting in an area of relative warming ($2^{\circ}C$) coincident with the low pressure area near (-9.5, -18). Relative warming is also found in the area southwest of the weak GF at (-16, -19.5). This warm area corresponds to the location of warm environmental air at the western edge of the storm. The warm-core structure microburst for the simple case at both analysis times is at variance with the cold-core microbursts for the complex case reported in Part I (Fig. 9). This result shows that the wet microburst with a weak down-flow will have a cold core since the evaporation of raindrops cools the air more effectively, especially in the area where the vertical velocity is very small or nearly zero. Conversely, the wet microburst with a strong downflow, observed in the simple case, will have a warm-core structure because embedded raindrops cannot evaporate fast enough to maintain a moist-adiabatic descent.

3.2 Vertical Cross-sectional Analysis

Fields of radar reflectivity (Z) with storm-relative winds superimposed and the V-component along line AB in Fig. 3a are shown in Fig. 7. This north-south cross section passes through the northern portion of the weak GF (heavy dashed line) and the microburst center (M). The vertical axis represents heights in kilometers AGL, while the horizontal axis indicates distances in kilometers from the microburst center (M). At the time of the analysis, the microburst was located 12.5 *km* west and 18 *km* south of the CP-2 radar. The microburst is embedded within the high reflectivity region ($Z > 40$ *dBZ*) with precipitation occurrence (Fig. 7a). It is characterized by a strong downflow from the 2 *km* height to the ground. As the rapidly descending air approaches the lowest layer near the ground, it begins to spread horizontally, forming a pronounced diverging outflow from the surface to 0.75 *km*. Strong wind shear develops along the outflow. Part of the outflow air moves from the microburst center (M) to the right (north), colliding with the environmental air at the storm's northern edge to form the GF. As a result, the buoyant environmental air is lifted, resulting in upward motion along the GF. A rotor is seen in the area

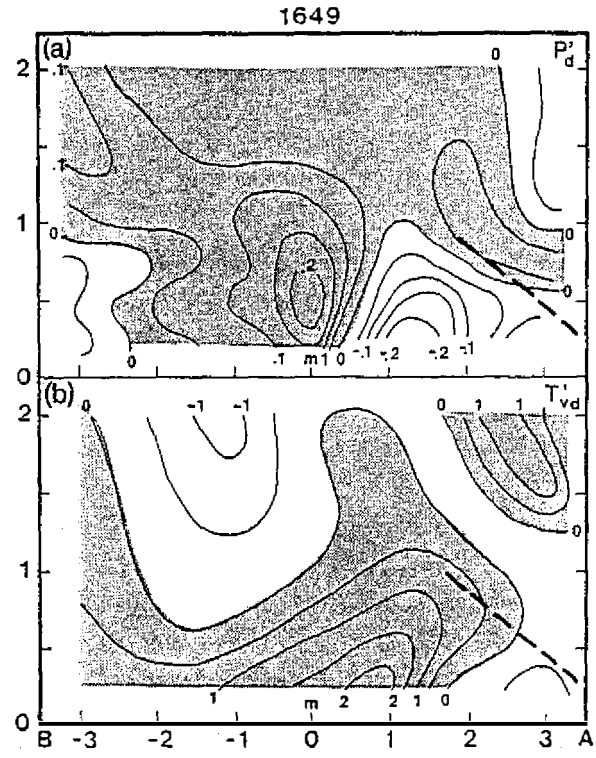

Fig. 9. The cross section along line AB in Fig. 3a showing (a) deviation perturbation pressure (P'_d), and (b) deviation perturbation temperature (T'_{vd}). Contour intervals are 0.5 *mb* and 0.5°*C* (with positive values shaded) for P'_d and T'_{vd}, respectively.

approximately 2 *km* north of M with the circulation center located near the 0.75 *km* height. This is caused by the interaction between the microburst outflow and incoming environmental flow. A similar feature was also found in Lin *et al.* (1987) for the same case but at 1647 MDT. The isotachs of the *V*-component are presented in Fig. 7b with positive values (northward) shaded. Note that the dominant outflow is confined to the level below 1 *km* with the maximum velocity differential of 12 m/s occurring below 0.5 *km*. It is in these lowest levels where strong low-latitude wind shear become critical to aircraft performance during take-off and landing (Fujita, 1985).

Figure 8 displays fields of vertical velocity and precipitation drag (PD) along the same cross section. An organized downdraft dominates the entire ABL, extending from the 2 *km* height to the surface. The maximum downdraft speed is about -5 m/s, which is much stronger than that observed at 1845 and 1850 MDT for the complex case (see Figs. 10 and 12 in Part I). However, it is weaker than the same downdraft observed two minutes earlier at 1647 MDT along the same cross section, see Fig. 7 in Lin *et al.* (1987) for comparison. This finding indicates that the microburst and its parent storm had begun to

weaken at 1649 MDT, showing the decaying stage of the storm's life cycle. In the shaded area north of M, upward motion dominates with maximum speed $> 4\ m/s$. As noted earlier, this updraft is caused by the presence of the GF over that area, which dynamically lifts the environmental air upward along the frontal surface. A cross-comparison between the w field (Fig. 8a) and reflectivity (Fig. 7a) reveals that the downdraft column matches well with strong reflectivities, shown the intimate relationship between the downdraft and precipitation loading. A similar feature was also found in Lin *et al.* (1987) for the same case at 1647 MDT. In order to know the role played by precipitation loading in affecting the net vertical acceleration, dw/dt, values of precipitation drag ($PD = -g\ q_r$) in units of $10^{-2}\ m/s/s$ are plotted in Fig. 8b. Recall in Part I Eq. (5), values of PD represent rainwater loading and were empirically estimated from radar reflectivities. In the buoyancy equation, the PD term always contributes negatively to the vertical acceleration, dw/dt. Examination of Fig. 8 reveals that contours of PD match well with isotachs of w in the downdraft. It is worth noting that the $2 \times 10^{-2}\ m/s/s$ contour for PD is equivalent to the rainwater mixing ratio (q_r) of $2\ g/kg$. Conversely, in the weak echo region, where the updraft dominates, the effect of rainwater loading is a minimum. This result shows that precipitation loading plays an important role in affecting the downdraft during the mature and decaying stages of the storm's life cycle.

Fields of P'_d and T'_{vd} along the same cross section are displayed in Fig. 9. As noted in Part I, the retrieved fields of pressure and temperature are the deviations from their horizontal average instead of the deviations from the environmental means. The unknown area means still vary with height. Hence, vertical cross sections of pressure and temperature must be carefully interpreted with the unknown means in mind. The pressure calculation (Fig. 9a) reveals that high pressure forms inside the microburst core. It is surrounded by low pressure to its left and right in the outskirt of the microburst. This low pressure is associated with the strong microburst outflow seen in Fig. 7a. A pronounced horizontal pressure gradient forms across the microburst to balance the accelerated flow at the lowest levels. Fujita (1985) suggested that there is a close relationship between the perturbation pressure and the horizontal wind in a microburst. Examination of Figs. 7b and 9a reveals that high pressure occurs in the weak wind region inside the microburst core, while low pressure forms in the strong outflow regions in the microburst outskirt. This finding is consistent with that reported in Fujita (1985). For these reasons, we believe that the pressure calculation presented in this study has a high level of confidence and the information derived is very useful. The microburst has a warm core as shown in Fig. 9b. As noted earlier, such warming is directly attributed to the rapidly descending air in the downdraft, which warms up nearly dry-adiabatically in

the surrounding with high relative humidity. This result is quite different from that for the complex case with much weaker downdrafts (see Figs. 11 and 13 in Part I). In the microburst outskirt near the GF, the cooling occurs since the downflow air there reduces its speed to practically zero in the surrounding with low relative humidity. As a result, the evaporative cooling overcomes the compressional warming over that region, resulting in a pronounced horizontal temperature gradient outward from the microburst center. A portion of the negatively buoyant air moves toward the north (right side of Fig. 9), interacting with the environmental air to sustain the GF over the northern edge of the storm. These processed would continue as long as the microburst outflow is present. In the area above the GF, the warming occurs inside the updraft. A secondary downdraft on the left side of the main downdraft is in the area of relative cooling. This weak downdraft has a comparably weak downflow (-2 m/s), as compared to the main downdraft (-5 m/s). As a result, the evaporative cooling prevails in that area, resulting in the temperature deficit of about $-1°C$. These results further reveal that the retrieved temperature field is closely related to the updraft-downdraft structure with warming in the updraft and cooling in the weak downdraft, in agreement with the observation reported in the literature. Like the retrieved pressure field, we believe that the retrieved temperature field has a high level of confidence as well in areas of high signal-to-noise ratio and small vertical wind shears. Therefore, useful information can be extracted from the retrieved fields.

3.3 Discussion

In the study by Lee *et al.* (1988), the evolution of a bow echo/microburst event was investigated using the JAWS Doppler data from 1526 to 1566 MST (equivalent to 1626 to 1666 MDT) 14 July 1982. The horizontal and vertical grid spacings were 0.4 and 0.8 km, respectively. Smoothing, vertical velocity and thermodynamic retrieval calculations were made in CEDRIC (Mohr *et al.*, 1986). Since their method of analysis is different from ours, it is of interest to compare their results at 1546 MST (1646 MDT) with ours at the same analysis time reported in the study by Lin *et al.* (1987), i.e., the simple case in the present study. A comparison was made between our lowest level (0.25 km AGL) to their lowest level (0 $\sim$ 150 m AGL), see their Fig. 3. It was found that the flow and reflectivity fields are very similar between the two studies. In the same manner, their vertical velocity (w) profile at heights below 5 km (see their Fig. 5) is also comparable to ours at the same heights (after the w-profiles in both studies were variationally adjusted to zero at the surface).

In regard to retrievals of perturbation pressure, their pressure field at 0.8 km agrees well with ours at 0.75 km. Furthermore, the reflectivity pattern between the two studies at this level is also comparable. For the retrieved

temperature field, our downdraft core at the 2 *km* level is found to be colder than its surrounding (see Figs. 10b and 11a in the study by Lin and Hughes, 1987). This finding is in agreement with that of Lee *et al.* (1988), except our temperature magnitude is slightly smaller than theirs.

The above comparisons reveal that the overall results between the two studies are quite consistent despite the fact that two different analysis techniques were employed in the studies. These findings further show that the structural features presented in both studies for the 14 July 1982 case are relevant and important.

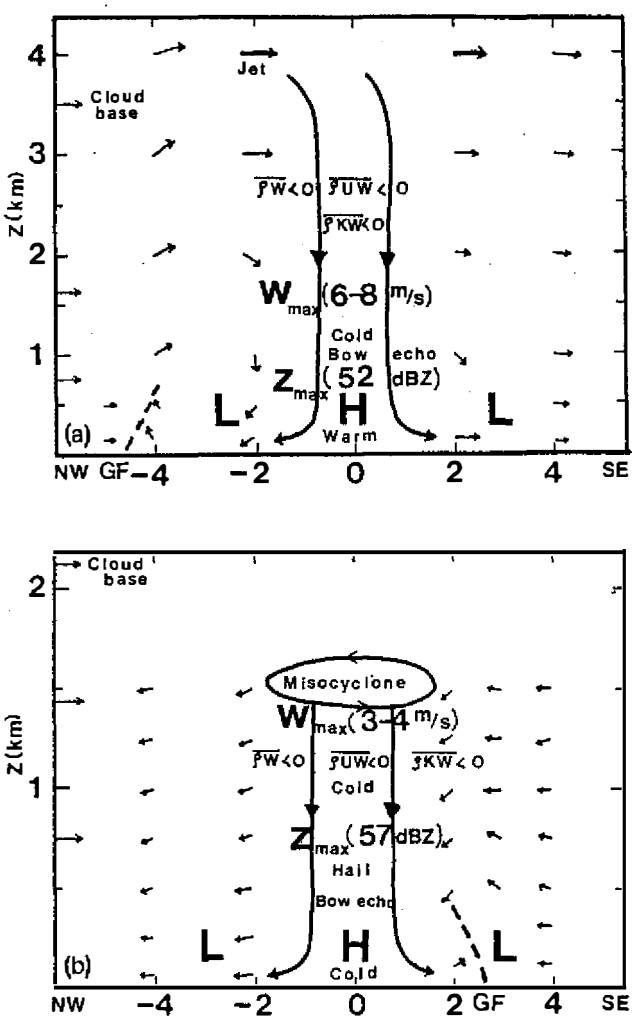

Fig. 10. A schematic diagram showing the important structural features of a microburst under investigation for the (a) 14 July case and (b) 5 August case. These features are extracted from the dual-Doppler data considered and are representative of the microburst structures at the times when the data were sampled.

4. HYPOTHESIZED CONCEPTUAL MODEL OF A MICROBURST

On the basis of the results presented in Part I and Part II of this study, we have hypothesized a microburst conceptual model during either the evolving or decaying stage of the storm. It must be pointed out that we are not attempting to show the entire evolution of a microburst due to the limited data sets considered in this investigaion. Instead, emphasis is placed on the structure of a microburst as revealed by dual-Doppler radars at the times when the data were sampled.

4.1 The Simple Case: 14 July 1982

The simple case (Fig. 10a) is characterized by a microburst embedded within a descending reflectivity core ($Z < 55\ dBZ$). The maximum downward vertical motion associated with the microburst was greater than 5 m/s. A bow echo circulation was present in this case with the microburst descending from near the head. The horizontal momentum and eddy kinetic energy budgets revealed the importance of the downward transport occurring from the subcloud layer. This result was also noted by Lin and Condray (1988) for the simple case at 1647 MDT. They also noted the presence of a 4 km jet. The strong wind shear near the 4 km jet ensures that a very turbulent environment prevails with eddy motion interacting with the downdrafts to produce downward transport of high-speed air. The dry high-speed air enters the bow echo from the rear, where it encounters the concave back edge of the bow echo. Mixing ensues, which creates precipitation-cooled air that transports the air downward. No well-organized misocyclone is present, because of the dominance of the larger scale winds and the lack of directional shear in the environmental winds. Srivastava (1987) has shown that microbursts may be initiated and maintained by dry entrainment processes. The key to this type of microburst seems to be the flux rate of high-speed, dry environmental air across the concave back edge of the bow echo. The greater the flux, the greater the mixing rate, which increases the downward transport of air. The rapidly descending air is compressionally warmed to create a warm core microburst, because of downward motion of 6 m/s or larger. This is a sufficiently rapid descent to not allow the saturated downdraft to mix with the environmental air. The air descends nearly dry adiabatically instead of moist adiabatically. These results were produced or observed in a simple one-dimensional model, Srivastava (1985, 1987); PAM station observations, Fujita (1985); and in a study using dual-Doppler data, Lin and Hughes (1987). The microburst centers were found to be centers of high perturbation pressure. The simple case is simple in part, because the larger scale flow can dominate the small scale flow; therefore, eddy motions of misocyclone circulations are suppressed or are of secondary importance, the microburst is

isolated with interactions limited to the outer edges of the microburst, and these types of storms can be predicted by techniques based on the presence of mid-level moisture and a deep, dry, well-mixed layer, Caracena *et al.* (1983). Of primary interest is what are the driving forces behind the complex case of a multiple microburst case that occurs in a microburst-producing storm not predicted by present forecasting techniques.

4.2 The Complex Case: 5 August 1982

The complex case (Fig. 10b) is characterized by several microbursts within a small domain. These storms interact with each other to produce gust fronts, rotor circulations, and they distort each other's outflow patterns. There are similarities with the simple case. The bow echoes do develop after the onset of the surface microburst. These bow echoes are aligned perpendicular to the mean environmental, high-speed air, associated with a low-level wind maximum. The microbursts are coincident with the high-reflectivity cores. Inflow into the bow echo, at levels above 1 *km*, is mixed with the saturated downdraft. Subsequently, the high-speed wind is collected above 1 *km*, then carried down to the surface layer of the microburst. The role of transport and buoyancy processes seems common to both types of microbursts. The microburst in a general conceptual model may be thought of as a mechanism for transporting mass, energy, and momentum, between the boundary layer and the subcloud/parent storm, which occurs above 1 *km*. A microburst is simply a very large organized turbulent eddy. The structural features responsible for the microburst development, and the physical processes that maintain them are not unique.

The structural features for the complex case feature a turbulent upper layer above 1 *km*, dominated by a misocyclone circulation, a weak divergent flow at 0.75 *km* that was dominated by the mean flow, and a very turbulent surface layer below 0.75 *km*, which was dominated by the microbursts and their secondary circulations. Of particular interest is the structure and development of the misocyclone at upper levels, and the microburst circulation at low levels.

The structure of the storm can be understood by examining how the microburst may have developed. The complex case is not conducive to forecasting, using techniques based on negative buoyancy from a deep, dry, mixed layer, see Caracena *et al.* (1983). Dry entrainment and evaporative cooling are not sufficient to initiate the microbursts for this type of storm. Precipitation loading is not the likely cause, because tropical and subtropical convection features heavy rains with comparatively and subtropical convection features heavy rains with comparatively mild horizontal surface winds. Hail has been noted within the core of microbursts, even within thunderstorms occurring in the moist gulf coast region. Wakimoto (1988) used dual-polarization data from the CP-2 radar to locate a 65 dBZ hail shaft within the microburst core. He suggested that the

presence of a hail shaft may be indicative of the presence of a microburst. Many researchers, including Hjelmfelt (1984) and Parsons *et al.* (1985), have noted that cyclonic circulations aloft are associated with appendages of very high reflectivity. Parsons *et al.* (1985) indicated that for a 30 June 1982 JAWS case, the microburst downdraft initially formed close to a small core of reflectivity embedded within a larger "arm" of reflectivity. An intense cyclonic circulation centered about a reflectivity appendage, with continuity to heights above cloud base, was noted by Hjelmfelt (1984). He also noted that peak surface reflectivities were attained prior to the maximum microburst divergence intensity. Also, evidence of low reflectivity notches in the neighborhood of the microburst downdrafts suggested that melting provides an additional source of energy. From a numerical model, Proctor (1988) showed that a warm core may be present. Hail is too small to compensate for compressional heating, unless the vertical velocity of the downdraft is very small. Since hail plays a relatively minor role in maintaining the microburst, its role may be in a different capacity. The main problem in distilling the answer from the evidence is to determine if the presence of the microburst is the result of the hail or the hail is the result of the presence of microburst. Hail falling in strong downdrafts has a significant advantage over hail that does not, in that it can spend considerably less time in the warm air before reaching the ground. A comparison of the 1649 MDT 14 July 1982 and the 1845, 1847 and 1850 MDT 5 August 1982 cases shows that cloud base is higher for the former case. The lower reflectivities encountered in the simple case suggests that the hail was incidental to the microburst. However, the complex case occurred in an environment of higher available latent heat for melting. Also, the downward motion within the microburst was one-half of the magnitude experienced in the simple case. This suggests that hail may be responsible in part for the microburst, since a larger volume of hail is necessary to maintain the high reflectivity values in the complex case, where the melting rate is higher, due to a slower descent of the hail in the microburst downdraft, relative to the simple case, and the greater availability of environmental latent heat. If there was another causal mechanism present, the reflectivity core should have been lower or the same as the simple case. We believe that a main causal mechanism for the complex case microburst was hail melt, but dry entrainment processes associated with the misocyclone circulation, precipitation drag, and downward momentum transport of energy extracted from the mean state to the eddy state maintained the microburst at lower levels. New forecasting techniques, to consider the role played by hail, are necessary to forecast microbursts for relatively moist soundings. By examining the conceptual model in a temporal sense, the microburst synthesis is clearer.

It is postulated that the evaporative cooling from precipitation initiates the downdraft (Srivastava, 1985), but the focus for the microburst is provided

by the descending hail shaft. The hail melt contributes the necessary additional negative buoyancy, when combined with evaporative cooling, to create a sufficient downward flux of mass and momentum to produce the microburst. The hail melts below the freezing level, with the maximum contribution of hail melt to negative buoyancy occurring at the bottom of the descending microburst. At that level, the melting is maximized, as the cool microburst air mixes with the warm subcloud layer. A commonly observed event with microbursts is a descending reflectivity core, accompanied by a "melting level depression". The contribution from hail melt to the microburst diminishes, once the microburst impinges on the surface. The air through the subcloud layer has been cooled; therefore, melting slows down with time. This is confirmed by the descending reflectivity core and the melting level depression. As the hail shaft becomes more insulated, the hail melt contribution to negative buoyancy is limited to the outer edge of the reflectivity core. Since hail melt no longer becomes a major factor in the microburst's development, some other mechanism must be evolving to take its place.

The misocyclone is not present during the early stages, as confirmed by M3 in the 5 August 1982 case. As the downdraft and microburst progress downward toward the surface, the atmospheric column, through which the downdraft descends, becomes stretched. The stretching occurs in a light wind environment of environmental winds less than 10 m/s, but with strong directional shear of the winds backing with height. Since the mesoscale forcing dominates the environment, the stretching of the vorticity initiates a cyclonic gyre above 0.75 km. The gyre entrains dry, high-speed, environmental air into the downdraft, where it mixes with the cool saturated downdraft. The enhanced dry entrainment with evaporative cooling, downward flux of momentum, and enhanced precipitation drag due to the precipitation core, become the primary maintainers of the microburst. The weak reflectivity notches, noted in this study, are a manifestation of this process. The evolution of the bow echo parallels the development of the misocyclone. In this study, the rotating head of the bow echo (Fujita, 1985) was coincident with the 1649 MDT case, and M1 of the 5 August 1982 case.

The surface microburst is a direct result of the downdraft impinging on a horizontal surface. The stretched downdraft becomes compressed as its downward velocity is slowed from contact with the ground. The compression results in a spin down of the downdraft. The cyclonic circulation undergoes spin down to a neutral condition at 0.75 km. Below that level, a rapid spin down creates a highly divergent circulation. The microburst sets up secondary circulations on its margins. A cat eye roll vortice forms on the outer edge of the microburst, when the horizontal shear between the microburst outflow opposes each other. The higher density flow will determine the sense of rotation. Interieri *et al.* (1988) used Doppler lidars to show that uneven flows produce gyres

and cat eye circulations. In addition, the gust front and environmental flow combine to create an updraft that stretches the surface vorticity to create a spinning updraft. At misocyclone levels, the misocyclone and mesocyclone-like circulation interact. The mesocyclone-like circulation facilitates the entrainment of environmental air into the misocyclone, thus becoming a feedback mechanism within the misocyclone/microburst circulation.

5. CONCLUSIONS

In Part II of this study, a comparison and cross-comparison in structure and internal dynamics is made between the simple case, which occurred on 14 July 1982, and the complex case on 5 August 1982. The simple case produced only a single microburst during the storm's life time. Conversely, the complex case produced at least two microbursts at each time of analysis. In both cases, dual-Doppler data collected during the JAWS project in Colorado were employed to derive the detailed wind fields using the same data analysis and reduction procedures. Subsequently, fields of deviation perturbation pressure and temperature were retrieved from the Doppler derived winds using the three momentum equations.

Results show that there are several similar and different features in structure and internal dynamics between the two cases. Similar features observed are: (1) all microbursts being investigated were embedded within the high-reflectivity regions with precipitation occurrence; (2) a wet microburst is accompanied by the bow echo with the diverging outflow in the direction nearly parallel to the maximum radar reflectivity; (3) high pressure occurs inside the microburst core with low pressure in the strongest outflow regions; (4) a rotor forms in the area near the microburst gust front due to the outflow colliding with the buoyant environmental flow; (5) a net transfer of horizontal momentum and eddy kinetic energy in the microburst area is predominantly downward; and (6) the pressure and buoyancy effects are two main contributors to the generation/decay of horizontal momentum fluxes and eddy kinetic energy at the microburst levels, having the same order of magnitude but opposite sign.

Different features between the two cases include: (1) each storm case has unique environmental ingradients, such as the wind, vertical shear, stability, and moisture; (2) the environmental mean flow in the ABL is opposite in direction (southest versus northwest); (3) a strong downflow ($6 \sim 8\ m/s$) occurs in the main downdraft for the simple case, while a relatively weak downdraft (about $3 \sim 4\ m/s$) prevails in the complex case; (4) only one microburst occurs in the simple case, while two to three microbursts form in the complex case; (5) no apparent circulation center is found in the simple case, while the complex case has the mesocyclone-like vortex and misocyclones; and (6) a wet microburst has a warm core for the simple case and a cold core for the complex case.

It must be pointed out that the above conclusions are reached based on only two cases of study. Additional studies are needed in the future to further understand the structure, internal dynamics, momentum transport, and energetics of a microburst-producing storm in Colorado and other geographical locations.

Acknowledgements. The authors wish to thank the National Center for Atmospheric Research (NCAR) for providing the dual-Doppler data and technical assistance. In particular, we are grateful to Kim Elmore of NCAR for his help in the preliminary data analysis and editing of the unified format data. Thanks also go to Robert Pasken and Robert Hughes for their assistance in computation. This research was partially supported by the Division of Atmospheric Sciences, National Science Foundation, under Grant ATM-8312172-01. J. A. Coover was supported by the Air Force Institute of Technology.

REFERENCES

Barnes, S., 1973: Mesoscale objective analysis using weighted time series observations, *NOAA Tech. Memo.* ERL-NSSL-62, 60 pp. (Available from National Severs Storms Laboratory, Norman, OK, 73069).

Caracena, F., J. McCarthy, and J. A. Flueck, 1983: Forecasting the likelihood of microbursts along the front range of Colorado, *Preprints, 13th Conference on Severs Local Storms*, Tulsa, Amer. Meteor. Soc., 261–264.

Fujita, T. T., 1985: The Downburst Microburst and Macroburst, *University of Chicago Press*, Chicago, 122 pp.

Gal-Chen, T., 1978: A method for the initialization of the anelastic equations: Implications for matching Models with observations, *Mon. Weather Rev.*, **106**, 587–606.

Hjelmfelt, M. R., 1984: Radar and surface data analysis of a microburst in JAWS, *Preprints, 22nd Conference on Radar Meteorology*, Zurich, Amer. Meteor. Soc., 64–69.

Intrieri, J. M., A. J. Bedard and R. M. Hadesty, 1988: Doppler lidar observaions of colliding outflow boundaries, *Preprints, 15th Conference on Severe Local Storms*, Baltimore, Amer. Meteor. Soc., 249–252.

Lee, W. C., R. E. Carbone, and R. M. Wakimoto, 1988: The evolution of a bow echo/microburst event in JAWS, *Preprints, 15th Conference on Severs Local Storms*, Baltimore, Amer. Meteor. Soc., 391–394.

Lin, Y. J., and R. G. Hughes, 1987: Structural features of a microburst-producing storm in Colorade revealed by JAWS dual-Doppler radars, *J. Atmos. Sci.*, **44**, 3640–3655.

Lin, Y. J., R. G. Hughes, and R. W. Pesken, 1987: Subcloud-layer kinematic and dynamic structure of a microburst-producing thunderstorm in Colorado determined from JAWS dual-Doppler measurements, *Boundary-Layer Meteorol.*, **39**, 67–86.

Lin, Y. J., 1988: The subcloud-layer eddy kinetic energy budget of a microburst-producing thunderstorm determined from JAWS dual-Doppler measurements, *Boundary-Layer Meteorol.*, **44**, 349–357.

Lin, Y. J., and P. M. Condray, 1988: Momentum flux in the subcloud layer of a microburst-producing thunderstorm determined from JAWS dual-Doppler data, *Boundary-Layer Meteorol.*, **43**, 125–141.

Lin, Y. J. and J. A. Coover, 1991: Observational study of a multiple microburst-producing storm. Part I: Kinematic, dynamic, and thermodynamic structures, TAO, **2**, 95–118.

Lin, Y. J., and J. A. Coover, 1990: Momentum and eddy kinetic energy transports by a multiple microburst-producing storm, *J. Geophy. Res.*, **95**, 7625–7636.

Mohr, C. G., L. J. Miller, R. L. Vaughn and H. W. Frank, The merges of mesoscale dataset into a common Cartesian format for efficient and systematic analysis, *J. Atmos. Ocean. Technol.*, **3**, 143–161.

Parsons, D. B., C. J. Kessinger, K. L. Elmore, and R. D. Roberts, 1985: An investigation into the forcing of microbursts, *Preprints, 14th Conference on Severe Local Storms*, Indianapolis, Amer. Meteor. Soc., 48–51.

Proctor, F. H., 1988: Numerical simulation of the 2 August 1985 DFW microburst with the three-dimensional terminal area simulation system, *Preprints, 15th Conference on Severe Local Storms*, Baltimore, Amer. Meteor. Soc., 99–102.

Srivastava, R. C., 1985: A simple model of evaporatively driven downdraft: Application to microburst downdraft, *J. Atmos. Sci.*, **42**, 1004–1023.

Srivastava, R. C., 1987: A model of intense downdrafts driven by the melting and evaporation of precipitation, *J. Atmos. Sci.*, **49**, 1752–1773.

Wakimoto, R. M., 1988: Operational aspects of a microburst-producing storm during MIST, *Preprints, 15th Conference on Severe Local Storms*, Baltimore, Amer. Meteor. Soc., 384–387.

產生微爆雷雨系統之觀測研究（二）單次微爆個案與多次微爆個案之比較

林永哲 John A. Coover, Jr.
美國聖路易大學 地球與大氣科學系
美國空軍氣象勤務中心

摘要

本文比較（科羅拉多州）單次微爆及多次微爆暴風雨的內部動力結構，而重點放至邊界層現象，其中包括了多都普勒風場及熱動力場的討論。

結果顯示，兩種狀況有相異之處也有相同之處。

相同的特性包括：

（1）微爆現象是包括於高回波降水區內。（2）濕的微爆伴隨弓形回波，外流之方向平行於最大回波強度梯度。（3）高壓存在於微爆之核心區，而低壓在最強外流區。（4）外流區產生垂直的渦流（rotor），其係因外流與環境相遇而生而。（5）在微爆現象內，水平擾動動量及動能向下傳遞。（6）壓力及浮力項是在微爆層內，產生及削減水平動量與擾動動能之主要貢獻者。

另一方面，不同處有：

（1）兩組各有不同之環境條件，如風向，風速，垂直風切，穩定度，及濕度等。（2）環境風風向相反。（3）單次微爆之下沈氣流區有很強的下降氣流，而多次微爆者之下降氣流則較弱。（4）單次微爆之狀況中，無明顯之環流中心，而多次微爆者則有中尺度氣旋。（5）單次微爆之狀況中，微爆核心爲暖濕，而多次微爆者則爲冷濕之核心。